Silicon (2023) 15:7489–7497
https://doi.org/10.1007/s12633-023-02601-5

RESEARCH

Next-generation Cost- Effective Photovoltaic Cell with Tailored Structural and Optical Properties of Silicon nanowires with Silver Nanoparticle Deposition

Savita Rani[1] · Rangeeta Dhaka[1] · A. K. Shukla[1]

Received: 19 April 2023 / Accepted: 13 July 2023 / Published online: 21 July 2023

Abstract
Metallic nanoparticles deposited semiconductor nanowires, a kind of heterostructures, show a remarkable property to strengthen optical and optoelectrical characteristics due to the coupling of surface plasmon with nanowires. The Silicon nanowires (SiNWs) are synthesized with metal-assisted chemical etching with different etching duration. Then silver nanoparticles (AgNPs) are deposited by the electroless deposition method over SiNWs, by maintaining the optimum deposition parameter. Here, the nanowire structures provided the flexibility to incorporate multiple metallic nanoparticles in a single system, which could have multiple applications in nanotechnology. Improved light absorption, increased surface area and enhanced charge carrier mobility make this substrate useful for next-generation photovoltaic cells. We experimentally measured the roughness of SiNWs and Ag-deposited SiNWs using atomic force microscopy, crystallite size using X-ray diffraction, optical reflectance by UV–visible spectroscopy, vibration and stretching of bonds by Fourier transform infrared spectroscopy and modified bandgap by photoluminescence spectroscopy. Our studies show that the change in the behaviour of SiNWs with deposition of AgNPs exhibits multifunctional properties, which can be of great significance in the field of nanowire solar cells, nanoelectronic devices, biological sensors, thermoelectric generators and high-efficiency photovoltaic cell.

Keywords Silver nanoparticles · Silicon nanowires · Electroless deposition · Metal-Assisted Chemical Etching

1 Introduction

Recently, the metallic nanoparticles deposited on semiconductors nanomaterials has gained traction in scientific communities, especially silicon nanowires (SiNWs), due to their excellent functionality and considerable potential for extensive application [1]. These metal nanoparticles serve as hot spots on the large area of the surface of the nanowires and also upgrade the optical and optoelectrical properties of the semiconductor nanowires [2]. The fabrication of silicon nanowires (SiNWs) can be done in various ways, both top-down and bottom-up. Among the most often used processes are vapour-liquid–solid growth [3], chemical vapour deposition [4], laser ablation [5], Thermal evaporation [6], and molecular beam epitaxy [7]. However, these techniques usually require complex equipment, high temperature, high vacuum and hazardous silicon precursor, all of which lead to an increase in the cost of processes. Therefore an elementary method, namely metal-assisted chemical etching (MACE) [8], has been proposed as a better alternative synthetic method to fabricate SiNWs.

Nanostructures with specific plasmonic properties and engineered surface functionalities have been fabricated by various approaches [9]. However, most of the reported literature on metal nanoparticles concerns the stabilization of metallic particles in aqueous media in the presence of a surfactant or water-soluble polymers as stabilizers. We have other methods like chemical vapour deposition / atomic layer deposition [10], thermal deposition method [11], hydrothermal methods [12] and femtosecond laser processing technique [13]. However, all these techniques are complex and tedious for feasible applications. The most schematic and economical is the electroless method [14]. Electroless deposition of metal nanoparticles is a productive way to decorate SiNWs with metallic nanoparticles such as Au or Ag [15].

✉ Savita Rani
phz188348@physics.iitd.ac.in

[1] Laser Assisted Material Processing and Raman Spectroscopy Laboratory, Department of Physics, Indian Institute of Technology, Hauz Khas, New Delhi 110016, India

Textured SiNWs surface with engineered nanoparticles can significantly enhance the light trapping effect, increases optical absorption and reduces surface reflection.

Additionally, Ag-deposited SiNWs heterostructures enhanced the interaction of photons with nanowires, resulting in outstanding photovoltaic capabilities. It also shows amplified photoconversion efficiency in photochemical solar cells. This heterostructure is unique in the interaction between surface plasmon resonances of Ag nanoparticles (AgNPs) and SiNWs. This leads to the amplification in the surface-enhance Raman signal. [16] AgNPs, on the other hand, have the highest molar extinction coefficient than any metal and also have the highest plasmonic efficiency, best electromagnetic enhancement, ideal optical properties, the highest molar Ag coefficient, highest levels of biocompatibility, chemical stability, and reactivity. Also, due to their versatility, they can be employed in sophisticated applications. [17].

In this paper, we show for the first time how the AgNPs deposited on SiNWs tailer the current density of substrate and amplify its usage in tunable photovoltaic cells. Also, study the change in the crystal behaviour, reflectance and bandgap after the deposition of AgNPs on SiNWs. After that, the modified behaviour of SiNWs etched for 20 min (SiNWs- 20 min), SiNWs etched for 30 min (SiNWs-30 min), Ag-deposited-SiNWs- 20 min and Ag- deposited- SiNWs- 30 min were analyzed with different characterization techniques. We contribute our latest results on enhanced optical and optoelectrical properties of SiNWs and Ag- deposited SiNWs. SiNWs- 20 min and SiNWs -30 show assertive crystalline behaviour after the AgNPs deposition. Strong anti-reflection properties and strong PL spectra are shown by SiNWs and Ag- deposited SiNWs. Our samples show intense stretching and vibrational modes in FTIR analysis. Current density is calculated by studying I-V characteristics. Our findings could consider the SiNWs and Ag-deposited SiNWs as promising candidates in optoelectronic applications and next-generation photovoltaic cells due to their distinctive structural, optical and electrical properties.

2 Experimental Details

2.1 Materials

HF (48%), acetone, $AgNO_3$ (98.9%), H_2O_2 (30%) were purchased from Thermofisher Scientific. Chemicals were used without futher purification.

2.2 Synthesis

Ag- deposited SiNWs are synthesized by MACE, followed by electroless deposition. The preparation method is based on Rani et al. [18]. Briefly, the etching solution of SiNWs is prepared by HF, H_2O_2, and DI in the ratio of 2:1:1. Then SiNWs are decorated with AgNPs to get the desired substrate for further analysis.

2.3 Characterization

With an accelerating voltage (20 kV), a scanning electron microscope (SEM) (Zeiss EVO 50) was used to examine the morphology of SiNWs. Transmission electron microscopy (TEM) (JEOL JEM-1400) was used to measure the diameter of SiNWs at a high accelerating voltage (120.0 kV). The silver-decorated SiNWs were removed from the sample for TEM by scratching them with a scalpel, and then they were collected and ultrasonically dispersed in 1 ml of ethanol. A little drop of the suspended solution was applied on a TEM copper grid, and it was air-dried before observation. The crystallography structures were determined by X-ray diffraction (XRD) using a Rigaku Ultima -IV X-ray diffractometer equipped with Cu Kα radiation ($\lambda = 1.54$ Å). A reflectance study was done using UV–Visible spectroscopy with a Perkin- Elmer UV–VIS-NIR spectrophotometer. Chemical analysis was done using Fourier Transform Infra-red spectroscopy (FTIR) with Thermo Scientific Nicolet Is 50 system. Photoluminescence spectra of the sample were recorded by an RF-6000 Shimadzer Spectroflorometer fitted with an excitation source with a particular excitation wavelength of 325 nm at room temperature.

3 Results and Discussion

Figure 1(a-d) presents SEM crossectional images for the as-grown SiNWs (a-b) and Ag- deposited SiNWs (c-d) etched for the time duration of 20 and 30 min, respectively. The uniform dispersal of the nanowires on the entire wafer and their verticle positions on the substrate surface was remarkably seen in cross-sectional images (a-b). The SiNWs length could be tuned from 11 μm to 20 μm by varying the etching duration from 20 to 30 min. As the etching time increases, the length of SiNWs increases, due to which absorption of light increases which leads to improved light harvesting efficiency in optoelectronic devices and also acts as a good scatter. Longer silicon nanowires have a large surface area, which can lead to enhanced capacitance and the ability to store more charge.

The spherical particles of silver nanoparticles of size 50 nm (approx.) distributed on the surface of nanowires are seen in Fig. 1 (c-d). The images show that the bundle-like structures are formed and ornamented with AgNPs. As illustrated in these figures, the diameter of AgNPs and interface roughness of the synthesized SiNWs and Ag- deposited SiNWs depend on the etching times and deposition

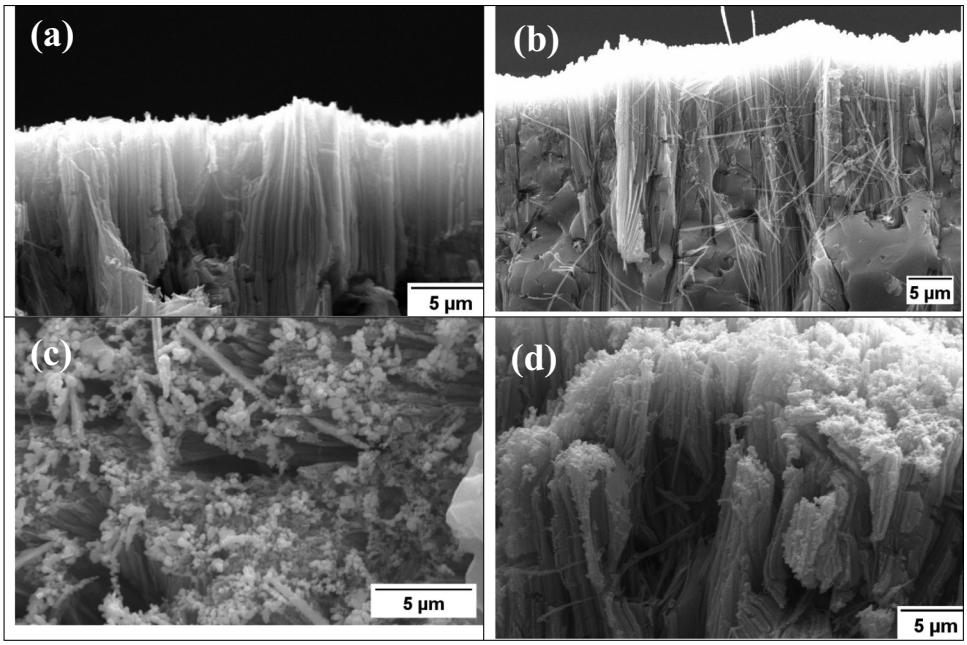

Fig. 1 SEM micrograph showing SiNWs- 20 min and SiNWs- 30 min using MACE technique in (**a**-**b**) respectively. Ag- deposited SiNWs- 20 min and Ag- deposited SiNWs- 30 min in (**c**-**d**) respectively

parameters of AgNPs. The deposition of AgNPs improves electrical conductivity, increases light absorption and scattering capability, and its usage as a photo-detector and solar cell. AgNPs also exhibit surface plasmon resonance and improved stability by acting as a protective layer and preventing the oxidation of silicon.

Figure 2(a-b) shows the TEM images of etched SiNWs for an etching duration of 20 and 30 min respectively. The average diameter remains constant at 55 nm (approx.) with increases in etching time from 20 to 30 min. The diameter of SiNWs depends on the AgNPs deposited on a silicon wafer which acts as a catalyst during the initial step of the MACE technique. Here the deposition parameter for AgNPs deposition is constant, due to which diameter remains almost the same for both the SiNWs [19].

Figure 3(a-d) shows the surface roughness and cross-sectional topography of SiNWs (a-b) and Ag- deposited SiNWs (c-d). The surface roughness (Ra) was estimated to be 170.93 nm and 311.36 nm for SiNWs with etching duration of 20 and 30 min respectively. Roughness increases with increases in etching time due to anisotropic etching, which is more pronounced along the < 100 > direction. Another factor, such as surface oxidation, selective etching and generation of dislocations with the increase in etching time, increases the roughness.

Ag-deposited SiNWs having Ra of 237.75 nm and 331.76 nm for etching duration of 20 and 30 min respectively. The Ra was estimated over a scope of 10 µm × 10 µm. It implies that the surface roughness is increased with AgNPs deposition. Here increase in roughness is due to the irregular shape and size of particles and also due to its non-uniform distribution pattern. The roughness of the surface

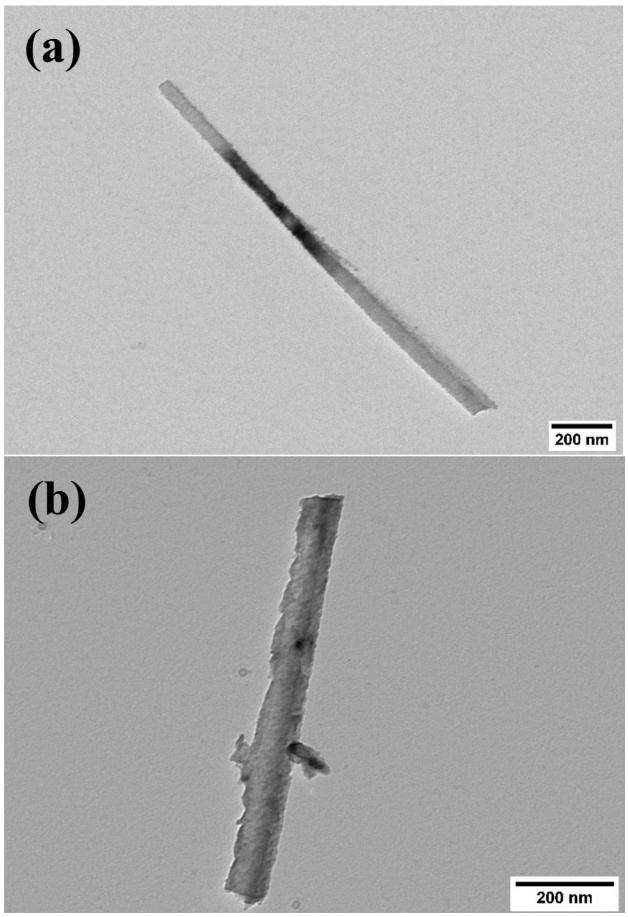

Fig. 2 (**a**-**b**) TEM images showing the diameter of SiNWs- 20 min and SiNWs- 30 min respectively

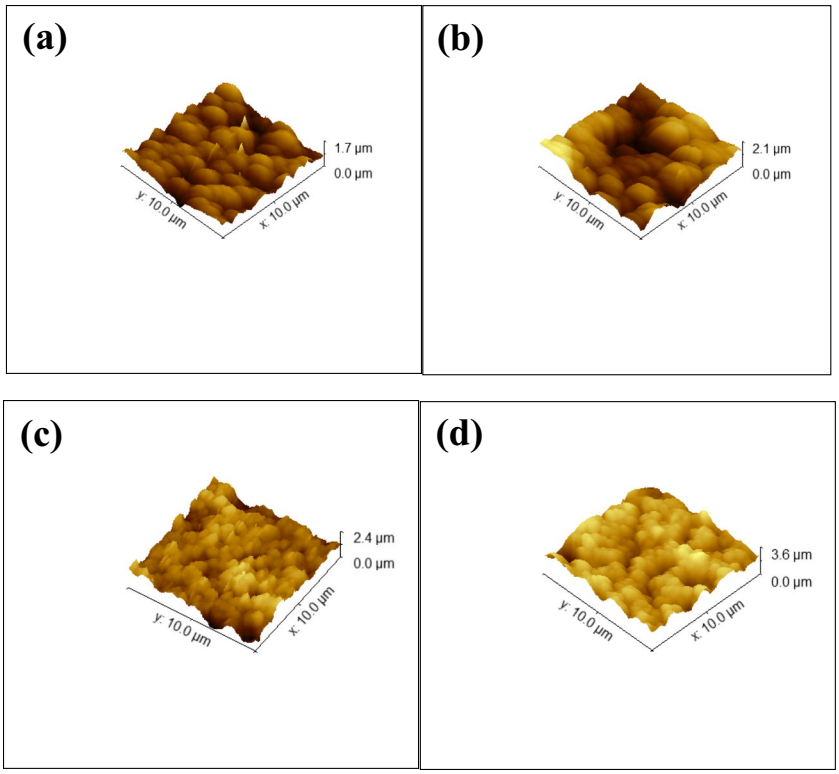

Fig. 3 AFM shows the roughness of the SiNWs- 20 min and SiNWs-30 min in (**a**-**b**) respectively and the roughness of Ag-deposited SiNWs- 20 min and Ag- deposited SiNWs- 30 min in (**c**-**d**) respectively

with the deposition of AgNPs increases the effective surface area, which increases light absorption.

The crystalline phase of the as-prepared sample is depicted using XRD in Fig. 4(a-c). A distinctive peak at 69 degrees that can be attributed to the (400) crystal plane of bare silicon in Fig. 4(a) demonstrates crystalline silicon structure. The primary silicon crystal structures can still be recognized on SiNWs after MACE processing, indicating that SiNWs and Ag-deposited SiNWs may be able to inherit the unique photochemical capabilities of silicon. No recognizable diffraction peaks of AgNPs can be recognized from the XRD pattern of Ag-deposited SiNWs in our case due to the low concentration and comparatively low diffraction intensity of AgNPs on SiNWs. [20]. The Scherrer formula [$D = K\lambda / \beta\cos\theta$] determines the crystallite size of SiNWs, where k is the instrumental correction factor. The calculated crystallite size of bare silicon, SiNWs with etching times of 20 and 30 min and Ag- decorated SiNWs with etching times of 20 and 30 min are given below in Table 1. We observed that bare Si in Fig. 4(a) show the highest crystalline behaviour. After an etching duration of 20 and 30 min, the crystallinity decreases, But after AgNPs deposition on SiNWs, there is a significant increase in crystalline behaviour in Ag- deposited SiNWs in Fig. 4(b-c). The crystallite size is increased with the etching duration from 20 to 30 min due to the slow etching rate alongside $<100>$ in wet chemical etching, causing the growth of larger crystal size. With the deposition of AgNPs, there is significant adhesion between the two material, which improve the size of the crystal. This implies that the crystallinity is improved after the deposition of AgNPs and improved in crystal size, increasing the conductive and absorption capability of the sample.

Figure 5(a) shows the UV- Visible reflection from a bare Si, which is 70 %. Figure 5(b) compares the reflection percentage of SiNWs -20 min and Ag-deposited SiNWs-20 min, which is reduced to 0.5 % after AgNPs deposition on SiNWs. Similarly, Fig. 5(c) shows that the reflection is decreased to 0.4 % after the deposition of AgNP on SiNWs-30. Fig.(d) shows the decrease in the reflectance with an increase in etching time from 20 min to 60 min etching time. It is due to increase in the density of SiNWs with an increase in etching in etching time from 20 to 60 min. However, the density of SiNWs is reduced by increasing the etching duration from 60 to 90 min due to the isotropic nature of wet chemical etching, which truncates the SiNWs and reduces the length and density of SiNWs. Thus, SiNWs etched for 90 min decrease the absorption and increase in reflectance of incoming light.

This implies that SiNWs surface with high absorption and thereby diminish the surface reflection due to the creation of features such as voids or pits that can trap the light. After the deposition of AgNPs, further reflection is reduced due to surface plasmon resonance (SPR). With electromagnetic wave excitation, AgNPs can be used as anti-reflection surfaces because they excite localized SPR that enhances the optical absorption by the light trapping. The internal

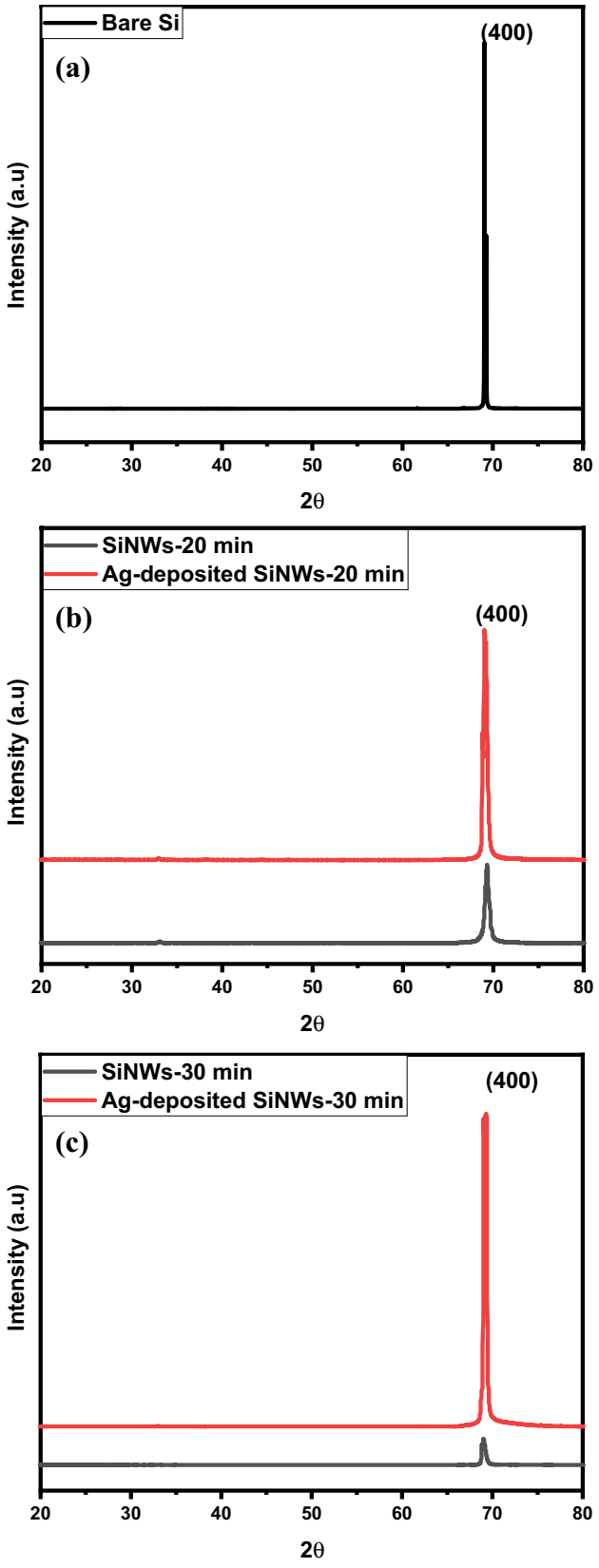

Fig. 4 XRD image of bare Si in (**a**), SiNWs- 20 min and Ag-deposited SiNWs-20 min in (**b**), SiNWs -30 min and Ag- deposited SiNWs- 30 min in (**c**)

Table 1 Crystallite size of SiNWs and Ag- deposited SiNWs calculated by XRD

S.NO	Sample name	Crystallite size (nm)
1	Bare Si	168
2	SiNWs-20 min	15
3	SiNWs-30 min	20
4	Ag- deposited SiNWs-20 min	18
5	Ag- deposited SiNW-30 min	22

scattering of light leads to a decrease in reflection [21]. Here combined properties of SiNWs and AgNPs are used, means a high aspect ratio with high etching time and surface plasmon resonance (SPR) of AgNPs are used. SPR effect induces the scattering of light inside the pores of nanowires and enhances the absorption of light. Another factor that makes our substrate suitable for photovoltaic cell as compared to other are its structure. That is synthesised at room temperature without any expensive techniques like lithography, pulse laser deposition and many other sophisticated techniques that require control temperature and pressure. Ag- deposited SiNWs are synthesised with chemical etching at room temperature to make it cost-effective for commercial application. By using these properties, SiNWs and Ag-deposited SiNWs can be better used in optoelectronic and photovoltaic devices.

Figure 6 shows the FTIR analysis to explore the surface composition of the as-prepared SiNWs and Ag- deposited SiNWs in (a-c). The spectra were collected in transmission mode in the spectral range of 500–3500 cm^{-1}. Three distinct vibration peaks can be seen on the bare Si wafer at 623 cm^{-1}, 1108 cm^{-1}, and 2087 cm^{-1}. The vibrational signature at 623 cm^{-1} reflects Si–O-Si stretching, SiOx and Si-H_2 stretching are shown by the vibrational fingerprints at 1108 and 2087 cm^{-1} respectively, here, x is equal to one or greater [22]. Si–O-Si stretching gets prominent with etching duration as shown in Fig. 6(b). With the deposition of AgNPs on SiNWs, the AS_1 vibration mode is responsible for peaks at 623 cm^{-1} and 1080 cm^{-1}, while AS_2 vibration mode is responsible for a shoulder at 1200 cm^{-1}. The presence of this shoulder is a characteristic of SiOx in sample. In Fig. 6(c), all the characteristic peaks of SiNWs are present after the etching of 30 min and after AgNPs deposition. The peak at 1200 cm^{-1} shows out-of-phase stretching of oxygen atoms, causing shoulder broadening. We notice that the surface states assigned to Si–O and Si–H chemical bonds are prevalent in all samples. Thus the presence of SiO_x in FTIR spectra of Ag-decorated SiNWs provides successful evidence of deposition of AgNPs.

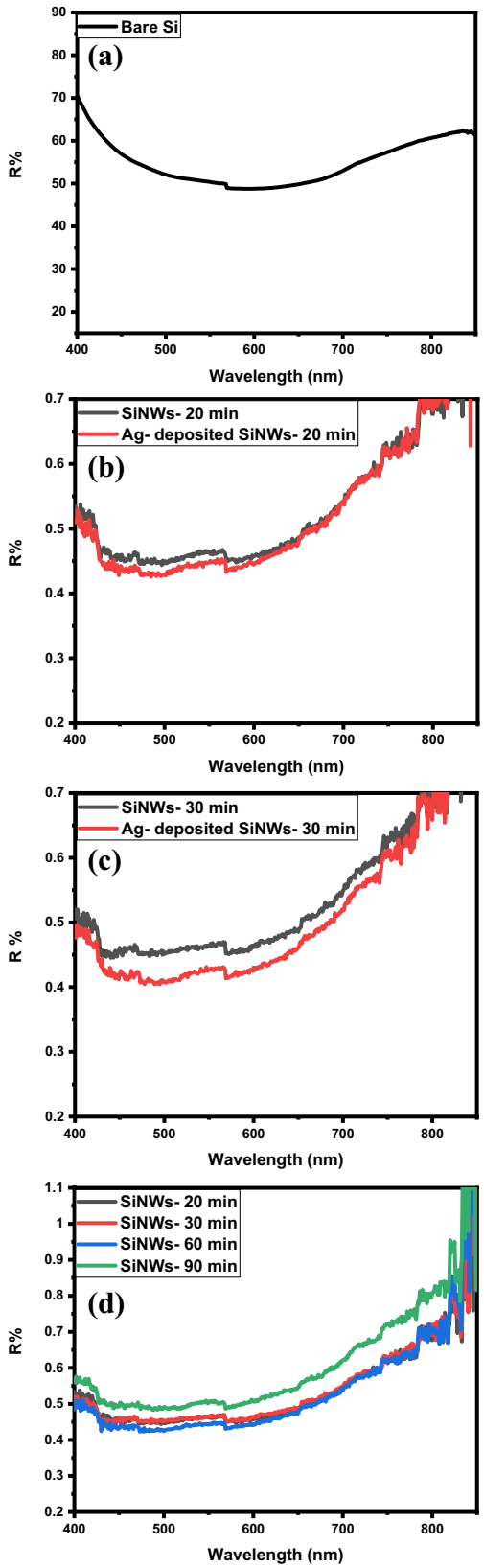

Fig. 5 UV- Visible spectra of bare Si in (**a**), SiNWs- 20 min and Ag-deposited SiNWs-20 min in (**b**), SiNWs-30 min and Ag-deposited SiNWs-30 min in (**c**) and SiNWs etched for 20, 30, 60, 90 min respectively in (**d**)

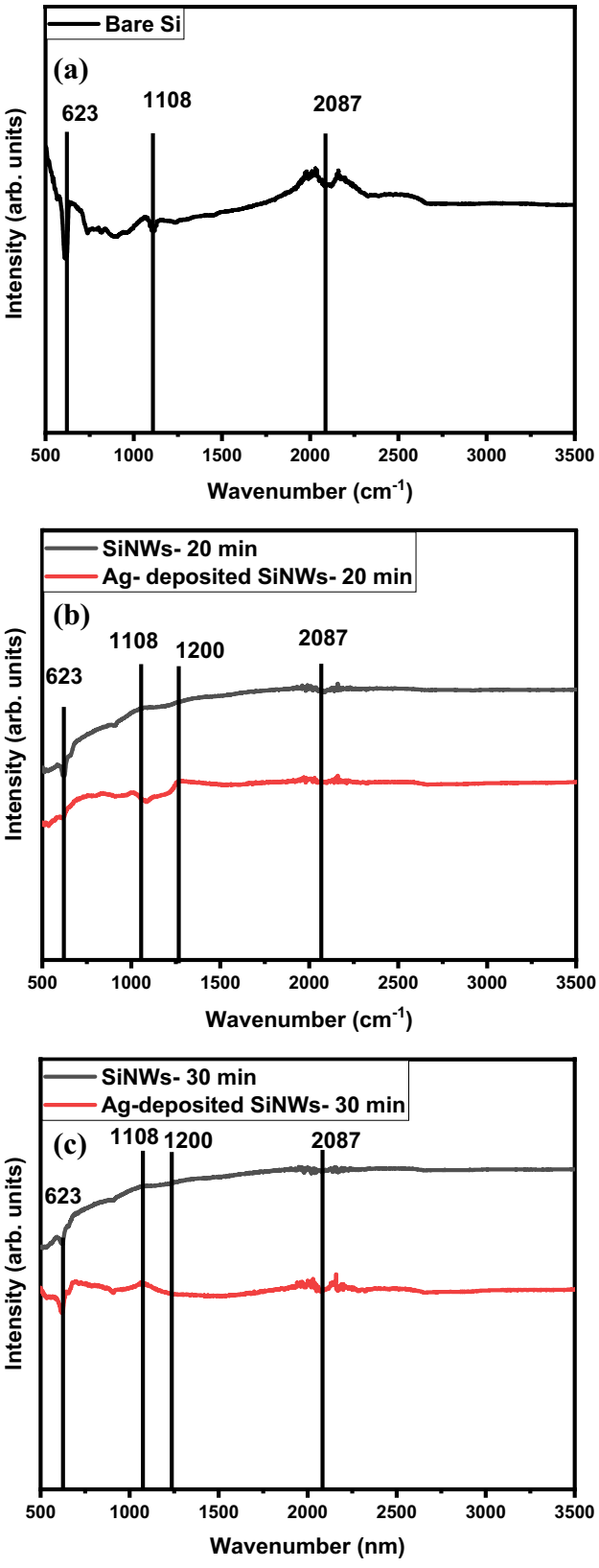

Fig. 6 FTIR spectra of bare Si in (**a**), SiNWs- 20 min and Ag-deposited SiNWs-20 min in (**b**), SiNWs-30 min and Ag-deposited SiNWs-30 min in (**c**)

Room temperature PL measurements of the as-synthesized samples were carried out in order to examine the effects of AgNPs deposition on SiNWs on PL properties. The origin of this PL emission has been explained by a number of mechanisms, including the quantum confinement (QC) effect and the existence of defects in a SiOx / Si interface or the surface of oxide connected to the Si–O-Si bonds [23]. According to numerous reports, the SiNWs have self-grown silicon nanocrystals (SiNCs) on them that are smaller than the silicon exciton Bohr diameter. At room temperature, these SiNCs shows strong quantum confinement results in strong PL spectra [24]. The PL spectra of SiNWs and Ag- deposited SiNWs are studied in detail in Fig. 7(a-b). Spectra corresponding SiNWs – 20 min in Fig. 7(a) confirm the peak at 823 nm and at 848 nm due to the different size distribution of silicon nanowires, which shows different band gaps. It is obvious that the PL intensity drops with the deposition of AgNPs. The surface coverages by AgNPs introduce the quenching effect, which hides the direct excitation of the SiNWs, and the reabsorption of the emitted light of SiNWs by AgNPs are two reasons that contribute to the decrease in PL intensity with the deposition of the AgNPs. Other factors include surface scattering, which decreases the PL intensity, and the interference effect due to AgNPs decreases PL intensity.

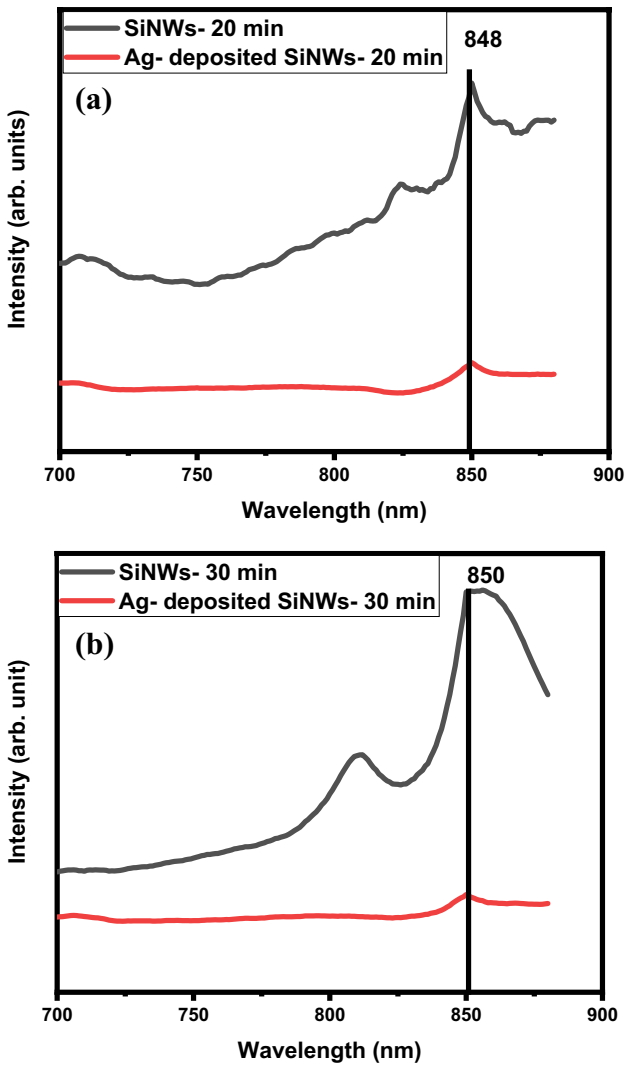

Fig. 7 PL spectra of SiNWs- 20 min and Ag-deposited SiNWs-20 min in (**a**), SiNWs-30 min and Ag-deposited SiNWs-30 min in (**b**)

Also, there is a Schottky connection between SiNWs and AgNPs, which causes the PL's intensity to diminish. The radiation recombination that results from the lowering of the PL can be limited by the potential interposed at the Schottky junction, which can also help with the systematic separation of photogenerated e–h pairs. Figure 7(b) shows similar PL spectra with a slight decrease in the bandgap of SiNWs with AgNPs deposition is given in Table 2. From the table, we observed the Ag- deposited SiNWs with an etching duration of 30 min have the minimum bandgap.

To understand the I-V characteristics and to determine the mechanisms of electrical transport in Ag- deposited SiNWs, Schottky junctions are formed by depositing a layer of chromium metal. A circular perforated mask of 1 mm in diameter was used to evaporate 100 nm of chromium metal. Electrical properties of SiNWs and Ag-deposited SiNWs samples are shown in Fig. 8(a-c) using current–voltage characteristics in daylight at room temperature in the voltage range -5 V to + 5 V with 20 mV step size. A rectifying behaviour of the curve due to contact of chromium metal electrode and silicon nanowires leads to the Schottky junction configuration, as shown in Fig. 8(a). Ag- deposited SiNWs- 30 min curve shows that current intensity decreases with increasing the etching time. The length of nanowires increases with etching which leads to a high ratio of surface area to volume that raises higher surface states. These surface states act as carrier trapping, which is responsible for lower current intensity in long nanowires. On the introduction of Ag nanoparticles on the surface of silicon nanowires, the

Table 2 The bandgap of SiNWs and Ag- deposited SiNWs was calculated by PL

S.NO	Sample	Absorption wavelength (nm)	Bandgap (eV)
1	SiNWs-20 min	848	1.468
2	Ag- deposited SiNWs- 20 min	848	1.468
3	SiNWs-30 min	850	1.464
4	Ag- deposited SiNWs- 30 min	850	1.464

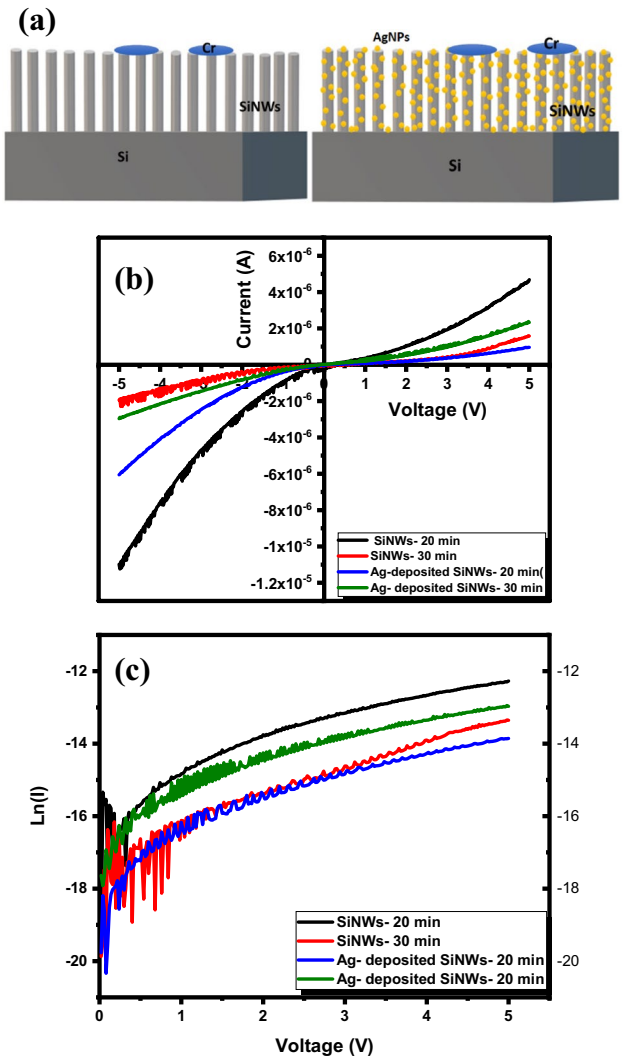

Fig. 8 Schematic of Schottky device in (**a**), I–V characteristics of the SiNWs and Ag- deposited SiNWs in (**b**) and Plot of Ln(I) vs voltage for SiNWs and Ag- deposited SiNWs in (**c**)

current density is influenced by the difference between the work function of silver (4.63 eV) and chromium (4.4 eV), which affect the Schottky barrier height, and AgNPs support the electron inflow due to the interface in between nanowires and electrodes. Electrical parameters

Table 3 The current density of SiNWs and Ag- deposited SiNWs was calculated by I-V characterstics

S.NO	Sample	I_s (Na)	η	φ_b(eV)
1	SiNWs-20 min	48.77	10.201	0.753
2	Ag- deposited SiNWs- 20 min	11.45	8.841	0.790
3	SiNWs-30 min	40.16	6.028	0.817
4	Ag- deposited SiNWs- 30 min	20.84	8.082	0.774

are calculated, shown in Table 3, using a thermionic emission model that expressed as

$$I = I_s\left[exp\left[\frac{q\left(V - IR_s\right)}{\eta kT}\right] - 1\right] \tag{1}$$

$$I_s = aA^*T^2exp\left[\frac{-q\varphi_b}{kT}\right] \tag{2}$$

where, ion current, q is the electronic charge, k is Boltzmann constant, T is the temperature, R_s is series resistance, η is the ideal factor, a is contact area of diode (0.0628 cm^2 in this case), A^* is Richardson constant (≈32 A cm^{-2} K^{-2} for p-Si) and φ_b is the Schottky barrier height.

At room temperature eV > > ηkT, that Eq. (1) can be considered as

$$I = I_s\left[exp\left[\frac{q(V)}{\eta kT}\right]\right] \tag{3}$$

On taking logarithmic on both sides of Eq. (2),

$$Ln(I) = Ln\left(I_s\right) + \frac{q(V)}{\eta kT} \tag{4}$$

Slope and intercept of the linear region of plot Ln(I) vs voltage shown in Fig. 8(c) used to calculate ideal factor and saturation current of the configuration, respectively. Saturation current value is used further to calculate the barrier height of configurations of metal Cr/SiNWs and Cr/Ag-deposited SiNWs [25].

Thus, the current density of SiNWs can be easily tuned with the increase in length and with the deposition of Ag-nanoparticle according to the need of substrate required. It has the great potential to be used as a photovoltaic cell due to localized surface resonance created by Ag- nanoparticles.

4 Conclusion

In summary, optically and electrically- active SiNWs and Ag- deposited SiNWs with strong PL emission, remarkable anti-reflection properties and fascinating electrical properties are systematically studied. Different characterization techniques are used to visualize the optical, structural, morphological and electrical properties of SiNWs and Ag-deposited SiNWs. Compared to the SiNWs, the formed Ag-deposited SiNWs demonstrate a high crystalline behaviour. The comparison of UV- Visible spectra of bare Si, SiNWs and Ag- deposited SiNWs shows a substantial reduction in reflectance to 0.4%. PL comparison of SiNWs and Ag-deposited SiNWs indicates that the PL intensity is decreased with AgNPs deposition. FTIR shows the basic stretching and

vibration modes are present after etching and after AgNPs deposition on SiNWs. I-V characteristics shows the tunable properties of SiNWs with Ag- nanoparticle deposition to fabricate photovoltaic cells. By showing that the Ag-deposited SiNWs are noticeably more optically and electrically productive than SiNWs, our research paves the road for their use in solar cells and optoelectronic devices.

Acknowledgements Thanks for the strong support from the Nanoscale Research Facility and Central Research Facility of IIT Delhi for characterization facilities and the Council of Scientific and Industrial Research New Delhi (CSIR).

Author Contribution Savita Rani: Conceptualization, Methodology, Writing-Original draft preparation, Visualization, Investigation, Validation, Result Analysis, Writing-Reviewing and Editing. Rangeeta Dhaka: I-V Result Analysis A.K. Shukla: Supervision, Reviewing and Editing.

Funding Savita Rani acknowledges the Council of Scientific & Industrial Research New Delhi grant number (09/086(1343)/2018-EMR-I) for financial support. All the other authors declare that no funds or support were received during this research work.

Data Availability The datasets generated during the current study are available from the corresponding author upon reasonable request.

Declarations

Competing Interests The authors declare no competing interests.

Consent for Publication Not applicable.

Consent for Participate Not applicable**.**

Ethics Approval Not applicable.

Competing Interest The authors have no relevant financial or non-financial interests to disclose.

References

1. Chen R et al (2012) Tailoring optical properties of silicon nanowires by au nanostructure decorations: Enhanced Raman scattering and photodetection. J Phys Chem C 116:4416–4422
2. Hutagalung SD, Fadhali MM, Areshi RA, Tan FD (2017) Optical and Electrical Characteristics of Silicon Nanowires Prepared by Electroless Etching. Nanoscale Res. Lett. 12:425
3. Wagner RS, Ellis WC (1964) Vapor-liquid-solid mechanism of single crystal growth. Appl Phys Lett 4:89–90
4. Demichel O et al (2009) Photoluminescence of silicon nanowires obtained by epitaxial chemical vapor deposition. Phys E Low-Dimensional Syst Nanostructures 41:963–965
5. Fukata N, Oshima T, Tsurui T, Ito S, Murakami K (2005) Synthesis of silicon nanowires using laser ablation method and their manipulation by electron beam. Sci Technol Adv Mater 6:628–632
6. Kumar RR, Rao KN, Phani AR (2012) Growth of silicon nanowires by electron beam evaporation using indium catalyst. Mater Lett 66:110–112
7. Xu T et al (2011) Synthesis of long group IV semiconductor nanowires by molecular beam epitaxy. Nanoscale Res Lett 6:1–7
8. Li X, Bonn PW (2000) Metal-assisted chemical etching in HF/H2O2 produces porous silicon. Appl Phys Lett 77:2572–2574
9. Watson KJ, Zhu J, Nguyen SBT, Mirkin CA (1999) Hybrid nanoparticles with block copolymer shell structures. J Am Chem Soc 121:462–463
10. Weimer AW (2019) Particle atomic layer deposition. J nanoparticle Res an Interdiscip forum nanoscale Sci Technol 21(9)
11. Nakano M, Fujiwara T, Koga N (2016) Thermal Decomposition of Silver Acetate: Physico-Geometrical Kinetic Features and Formation of Silver Nanoparticles. J Phys Chem C 120:8841–8854
12. Kim M et al (2014) Hydrothermal synthesis of metal nanoparticles using glycerol as a reducing agent. J Supercrit Fluids 90:53–59
13. Betancourt-Galindo R et al (2014) Synthesis of copper nanoparticles by thermal decomposition and their antimicrobial properties. J Nanomater 2014:7–11
14. Zhu J, Kim K, Liu Z, Feng H, Hou S (2014) Electroless Deposition of Silver Nanoparticles on Graphene Oxide Surface and Its Applications for the Detection of Hydrogen Peroxide. Electroanalysis 26:2513–2519
15. Rao GPC, Tharmaraj V, Yang J (2015) Surfactant-assisted electroless deposition of silver nanoparticles on Ge crystal for ultrasensitive detection by surface-enhanced infrared absorption spectroscopy. RSC Adv 5:20390–20395
16. Liao W, Liu K, Chen Y, Hu J, Gan Y (2021) Au–Ag bimetallic nanoparticles decorated silicon nanowires with fixed and dynamic hot spots for ultrasensitive 3D SERS sensing. J Alloys Compd 868:159136
17. Mahmud S et al (2019) Tailored Engineering of Bimetallic Plasmonic Au@Ag Core@Shell Nanoparticles. ACS Omega 4:18061–18075
18. Rani S, Shukla AK (2021) Investigation of silver decorated silicon nanowires as ultrasensitive and cost-effective surface-enhanced Raman substrate. Thin Solid Films 723:138595
19. Leonardi A, Faro A, Lo MJ, Irrera A (2021) Silicon nanowires synthesis by metal-assisted chemical etching: A review. Nanomaterials 11:1–24
20. Meng H, Fan K, Low J, Yu J (2016) Electrochemically reduced graphene oxide on silicon nanowire arrays for enhanced photoelectrochemical hydrogen evolution. Dalt Trans 45:13717–13725
21. Xu L, Li F, Liu Y, Yao F, Liu, S (2019) Surface Plasmon Nanolaser: Principle, Structure, Characteristics and Applications. Applied Sciences 9
22. Zamchiy AO et al (2018) Deposition time dependence of the morphology and properties of tin-catalyzed silicon oxide nanowires synthesized by the gas-jet electron beam plasma chemical vapor deposition method. Thin Solid Films 654:61–68
23. Sivakov VA, Voigt F, Berger A, Bauer G, Christiansen SH (2010) Roughness of silicon nanowire sidewalls and room temperature photoluminescence. Phys. Rev. B - Condens. Matter Mater. Phys. 82:1–6
24. Ghosh R, Pal A, Giri PK (2015) Quantitative analysis of the phonon confinement effect in arbitrarily shaped Si nanocrystals decorated on Si nanowires and its correlation with the photoluminescence spectrum. J Raman Spectrosc 46:624–631
25. Rouis A, Hizem N, Hassen M, Kalboussi A (2022) Electrical Properties of Silicon Nanowires Schottky Barriers Prepared by MACE at Different Etching Time. Silicon 14:4731–4737